MECSOL 2019 - Proceedings of the 7th International Symposium on Solid Mechanics,
V. Tita, A. Ferreira, M.L. Ribeiro, A. Vieira and A.T. Beck (Editors), ABCM, Sao Carlos, SP, Brazil, April 15th to 17th, 2019

MECSOL 2019 - Nonlinear Analysis of Functionally Graded Axisymmetric Structures under Thermal Environment

José Moita [1], Cristóvão Mota Soares [1], and José Herskovits [2]

[1] IDMEC, Instituto Superior Técnico, Universidade de Lisboa, Av. Rovisco Pais, 1049-001, Lisboa, Portugal

[2] COPPE-UFRJ, Universidade Federal do Rio de Janeiro, Rio de Janeiro, Brasil

Abstract: In this work is presented the formulation for static analysis of functionally graded axisymmetric plate/shell type structures subjected to axisymmetric mechanical loading under thermal environment. The formulations accounts for linear, geometric and material nonlinear behaviours. A finite element model is implemented and is based on a simple conical frustum finite element with 2 nodes, and 3 degrees of freedom per node, and it shows to be extremely efficient in the analysis of axisymmetric shells subjected to axisymmetric loading. The solution of some illustrative pressure vessel examples are presented and discussed.

Keywords: Functionally Graded Materials, Finite Element, Nonlinear Analysis, Elastoplasticity.

INTRODUCTION

Structures made of Functionally Graded Material (FGM) are characterized by a continuous variation of the material properties over the thickness direction by mixing two different materials, metal and ceramic. Ceramic with the low thermal conductivity can resist high thermal environment while metal is strong with mechanical load. Also, the smooth and continuous variation of the properties from one surface to the other eliminates abrupt changes in the stress and displacement distributions, and it allows the metal–ceramic FGM structures to be widely used in aircraft, space vehicles, reactor vessels, and other engineering applications.

Research in FGM structures has been done in the recent years. In nonlinear analysis of FGM axisymmetric plates, some works had been published. Here, we cite the works of "Reddy et al. (1999)" that using the Mindlin plate theory, study the axisymmetric bending of through-the-thickness functionally graded circular plates; "Ma et al. (2008)" that analyse the axisymmetric nonlinear bending behaviour of functionally graded circular plates, under mechanical and thermal loading; "Gunes and Reddy (2008)" that present the geometrically nonlinear analysis of functionally graded circular plates; "Li et al. (2008)" that study by the stress function method, the problem of transversely isotropic functionally graded materials plates with simply supported or clamped edge, subject to a transverse load.

Elastoplasticity analysis has been little investigated in FGM structures. Most of the published works involves plate/shells structures made of isotropic materials. For axisymmetric structures, in particular, "Kirk and Gill (1975) presented experimental results for limit pressures and instability failure, and compare these results with theoretical values; Zhang and Zhou (2015)" presented a model for FGM circular plates based on a physical neutral surface and a higher-order shear deformation theory.

The mechanical properties of FGM are dependent not only of the p-index of the power-law that defines the volume fractions of ceramic and metal phases, but can also be dependent of the temperature environment. In this paper is presented the static bending analysis of functionally graded axisymmetric plate-shell type structures subjected to axisymmetric loading. The formulation accounts for linear, elastoplastic and geometric nonlinear behaviours, and includes the global response of the plate-shell structures, the through-thickness stress distribution and the effective stress calculations, involving the variation of volume fractions and temperature environment. The solutions are obtained using a finite element model proposed by "Zienckiewics et al. (1977)", the conical frustum, which is a simple finite element with 2 nodes, and 3 degrees of freedom per node, and used a reduced Gauss integration technique. As it is necessary few elements to model the geometry of axisymmetric shells using this finite element, it reveals to be extremely efficient. An in-house finite element code had been implemented, and the solutions for some illustrative example are presented and discussed.

FORMULATION OF FGM MODEL

The material properties of an FGM plate/shell structure are assumed to change continuously throughout the thickness

only, according to the volume fractions of the constituent materials, which are ruled by a Power-Law function, "Bao and Wang (1995)". In this work, the continuous variation of the materials mixture is approximated by the using of a certain number of virtual layers throughout the thickness direction - layer approach. Thus, the volume fractions for each virtual layer are:

$$V_c^k = \left(0.5 + \bar{z}_k / h\right)^p \quad ; \quad V_m^k = 1.0 - V_c^k \tag{1}$$

where h is the thickness of structure, the exponent p a parameter that defines gradation of material properties across the thickness direction, and $\bar{z}_k$ is the thickness coordinate of mid-surface of each layer.

For the case of the temperature-dependent material properties, the properties of each constituent are obtained as follows, "Javaheri and Eslami (2002)":

$$\begin{Bmatrix} E\ (T) \\ \nu\ (T) \\ \alpha\ (T) \end{Bmatrix} = \begin{Bmatrix} E\ (T_0) \\ \nu\ (T_0) \\ \alpha\ (T_0) \end{Bmatrix} \left(P_{-1} / T + 1 + P_1 T + P_2 T^2 + P_3 T^3\right) \tag{2}$$

where $T = T_0 + \Delta T$, T_0 = 300 K (ambient, stress free temperature), P_{-1}, P_1, P_2, P_3 are the coefficients of temperature (in Kelvin), unique to each constituent, and ΔT is the temperature change.

Once the volume fractions V_c^k and V_m^k have been defined, the material properties of each virtual layer k, of an FGM can be determined by the rule of mixtures, coming

$$E_k(T) = V_c^k\ E_c(T) + V_m^k\ E_m(T)\ ;\ \nu_k(T) = V_c^k\ \nu_c(T) + V_m^k\ \nu_m(T)\ ;\ \alpha_k(T) = V_c^k\ \alpha_c(T) + V_m^k\ \alpha_m(T) \tag{3}$$

DISPLACEMENT AND STRAIN FIELDS.

For axisymmetric shells subjected to axisymmetric loading is $u_\theta = 0$. The displacement of a point on the meridian plane, is uniquely determined by two components u and w in the tangential (s) and normal (n) directions, respectively.

$$\begin{Bmatrix} u(s,n) \\ w(s,n) \end{Bmatrix} = \begin{bmatrix} 1 & 0 & -z \\ 0 & 1 & 0 \end{bmatrix} \begin{Bmatrix} u_0 \\ w_0 \\ \beta \end{Bmatrix} \ ;\ \mathbf{u} = \mathbf{Z}\,\mathbf{d} \tag{4}$$

where u_0, w_0 are displacements of a generic point in the mid-surface referred to the local axes, and β is the rotation of the normal to the middle plane, and can vary independently.

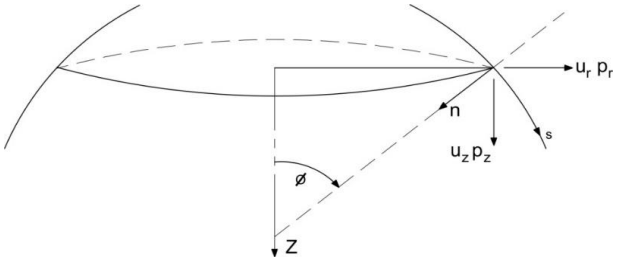

Fig. 1- Axisymmetric shell.

As we are considering a straight finite element, thus, the radius of curvature is $R = \infty$. Also is $u_\theta = 0$ and $d/d\theta = 0$. Then, the linear strains in the local system are given by:

$$\begin{Bmatrix} \varepsilon_s^0 \\ \varepsilon_\theta^0 \\ \kappa_s \\ \kappa_\theta \\ \gamma_{sn} \end{Bmatrix} = \begin{Bmatrix} du/ds \\ (u\cos\phi - w\sin\phi)/r \\ -d\beta/ds \\ -\beta\cos\phi/r \\ dw/ds - \beta \end{Bmatrix} \tag{5}$$

The relations between local (s,n) and global (r,z) coordinates as well as local-global displacements are given by:

$$\begin{Bmatrix} s \\ n \end{Bmatrix} = \begin{bmatrix} \cos\phi & \sin\phi \\ -\sin\phi & \cos\phi \end{bmatrix} \begin{Bmatrix} r \\ z \end{Bmatrix} \quad ; \quad \begin{Bmatrix} u_0 \\ w_0 \end{Bmatrix} = \begin{bmatrix} \cos\phi & \sin\phi \\ -\sin\phi & \cos\phi \end{bmatrix} \begin{Bmatrix} u_r \\ u_z \end{Bmatrix} \tag{6}$$

Thus the linear strain components in the global coordinate system come:

$$\begin{Bmatrix} \varepsilon_s^0 \\ \varepsilon_\theta^0 \\ \kappa_s \\ \kappa_\theta \\ \gamma_{sn} \end{Bmatrix} = \begin{Bmatrix} (\partial u_r / \partial s)\cos\phi + (\partial u_z / ds)\sin\phi \\ u_r / r \\ -d\beta_r / ds \\ -(\beta_r \cos\phi)/r \\ -du_r / ds)\ \sin\ \phi + (du_z / ds)\ \cos\ \phi - \beta \end{Bmatrix} \tag{7}$$

The stress-strain relations, in elastic behaviour, for each virtual layer k, can be written as:

$$\boldsymbol{\sigma}_k = \mathbf{Q}_k\ \boldsymbol{\varepsilon}_k \tag{8}$$

where $\boldsymbol{\sigma}_k = \{\, \sigma_s \quad \sigma_\theta \quad \tau_{sn} \,\}^T$ is the stress vector and $\boldsymbol{\varepsilon}_k = \{\, \varepsilon_s \quad \varepsilon_\theta \quad \gamma_{sn} \,\}^T$ is the strain vector, $\mathbf{Q}_k$ is the elasticity matrix for isotropic materials:

$$\mathbf{Q}_k = \begin{bmatrix} \dfrac{E_k}{1-\nu^2} & \dfrac{\nu E_k}{1-\nu^2} & 0 \\ \dfrac{\nu E_k}{1-\nu^2} & \dfrac{E_k}{1-\nu^2} & 0 \\ 0 & 0 & \dfrac{5}{6}\dfrac{E_k}{2(1+\nu_k)} \end{bmatrix} \tag{9}$$

Due to no symmetric grading of the material through the thickness, the bending-stretching coupling exists. Thus, the constitutive equation is given by:

$$\begin{Bmatrix} \mathbf{N} \\ \mathbf{M} \\ \mathbf{Q} \end{Bmatrix}_k = \begin{bmatrix} \mathbf{A} & \mathbf{B} & \mathbf{0} \\ \mathbf{B} & \mathbf{C} & \mathbf{0} \\ \mathbf{0} & \mathbf{0} & \mathbf{A}_s \end{bmatrix}_k \begin{Bmatrix} \boldsymbol{\varepsilon}^m \\ \boldsymbol{\varepsilon}^b \\ \boldsymbol{\varepsilon}^s \end{Bmatrix}_k \quad ; \quad \tilde{\boldsymbol{\sigma}}_k = \hat{\mathbf{D}}_k\ \boldsymbol{\varepsilon}_\kappa \tag{10}$$

where $\hat{\boldsymbol{\sigma}}_k$ are the resultant forces and moments, and $\hat{\mathbf{D}}_k$ the constitutive matrix, and

$$(\mathbf{A},\mathbf{B},\mathbf{C})_k = \mathbf{Q}_k \int_{z_{k-1}}^{z_k} (1, z, z^2)\, dz \quad ; \quad \mathbf{A}_{sk} = \mathbf{Q}_k \int_{z_{k-1}}^{z_k} dz \tag{11}$$

ELASTO-PLASTIC FORMULATION FOR FGM STRUCTURES

The present work uses an extended Tamura–Tomota–Ozawa (TTO) model to describe the elastic–plastic behaviour of ceramic/metal FGM. Ceramic materials are, in general, brittle materials of relatively higher elastic modulus and strength than those of metallic materials, which have typically ductile properties. Thus, the ceramic constituent in FGM is assumed to be elastic when deformation takes place. The elasto-plastic deformation occurs mainly by the plastic flowing of the metallic constituent. The TTO model, or also called the modified rule-of-mixture, uses the stress-strain transfer parameter q, which depends on the constituent material properties and the microstructural interaction in the FG material, and is given in "Jin et al. (2003)":

$$q = (\sigma_1 - \sigma_2) / |\varepsilon_1 - \varepsilon_2| \tag{12}$$

Using this parameter, the variation through the thickness of Young's modulus and the yield stress, σ_Y, may be obtained as follows:

$$E^k = \left(V_m^k E_m \frac{q + E_c}{q + E_m} + V_c^k E_c \right) \Bigg/ \left(V_m^k \frac{q + E_c}{q + E_m} + V_c^k \right) \tag{13a}$$

$$\sigma_Y^k = \sigma_{Ym}\left(V_m^k + \left(\frac{q+E_m}{q+E_c}\right)\frac{E_c}{E_m}V_c^k\right) \tag{13b}$$

Elasto-plastic constitutive relation

To carry out elastoplastic analysis, the material is assumed to obey the von-Mises yield criterion, and the corresponding yield surface is assumed. The yield condition can be expressed as, "Nayak and Zienckiewics (1972)":

$$F(\sigma,\kappa) = f(\sigma) - \sigma_Y(\kappa) = 0 \tag{14}$$

where the yield level, σ_Y, can be a function of the hardening parameter κ.

For the case of an isotropic material, and for the specific structures analysed here, the effective stress $\bar{\sigma}$ is given by:

$$f(\sigma) = \bar{\sigma}^2 = (\sigma_s)^2 + (\sigma_\theta)^2 - (\sigma_s\ \sigma_\theta) + 3(\tau_{sn})^2 \tag{15}$$

The elasto-plastic increments of total strains can be calculated by summing up the elastic and the plastic strain components:

$$d\,\varepsilon = d\,\varepsilon^e + d\,\varepsilon^p \tag{16}$$

The plastic strain increment is defined as proportional to the stress gradient of a plastic potential, which is taken equal to the yield surface condition for an associated flow rule. Following the development described in "Moita et al. (2016)", an incremental constitutive elastoplastic relation is obtained, through an elastoplastic constitutive matrix:

$$d\boldsymbol{\sigma} = \mathbf{Q}^{ep}\ d\boldsymbol{\varepsilon}\ \ ;\ \ \mathbf{Q}^{ep} = \mathbf{Q} - \frac{\mathbf{Q}\,\mathbf{a}\,\mathbf{a}^T\mathbf{Q}}{A + \mathbf{a}^T\mathbf{Q}\,\mathbf{a}} \tag{17}$$

where $\mathbf{a} = dF/d\sigma$ and $A = d\bar{\sigma}/d\varepsilon^p$ are the flow vector and the hardening parameter, respectively.

FINITE ELEMENT APPROACH

In the present work is used a conical frustum – straight finite element, Fig. 2, with 2 nodes and 3 degrees of freedom per node, the displacements and rotation, $u_{ri}, u_{zi}\ \beta_i$. The simplest interpolation functions for an element are:

$$N_1 = (1-\xi)/2\ \ ;\ \ N_2 = (1+\xi)/2 \tag{18}$$

$$\xi = \mp 1\ \ ;\ \ \xi = 2s/L\ \ ;\ \ 2\,ds = L\,d\xi \tag{19}$$

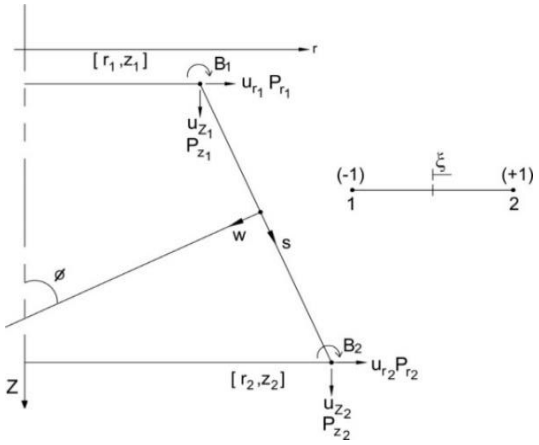

Figure 2 – Conical frustum element

The nodal displacement vector is then given by:

$$\begin{Bmatrix} u_r \\ u_z \\ \beta \end{Bmatrix} = \sum_{i=1}^{2} \begin{bmatrix} N_i & 0 & 0 \\ 0 & N_i & 0 \\ 0 & 0 & N_i \end{bmatrix} \begin{Bmatrix} u_{ri} \\ u_{z_i} \\ \beta_i \end{Bmatrix} \quad ; \quad \mathbf{u}=\mathbf{N}\,\mathbf{a} \quad ; \quad \mathbf{u} = \sum_{i=1}^{2} \mathbf{N_i}\ \mathbf{d}_i , \tag{20}$$

The linear strain vector $\boldsymbol{\varepsilon}_k = \left\{ \varepsilon_s \quad \varepsilon_\theta \quad \kappa_s \quad \kappa_\theta \quad \gamma_{sn} \right\}_k^T$ can be represented by: $\boldsymbol{\varepsilon} = \mathbf{B}\,\mathbf{a}$; $\boldsymbol{\varepsilon} = \sum_{i=1}^{2} \mathbf{B_i}\ \mathbf{d}_i$, where $\mathbf{B}_i$ is:

$$\mathbf{B}_i = \begin{bmatrix} \frac{dN_i}{ds}\cos\phi & \frac{dN_i}{ds}\sin\phi & 0 \\ \frac{N_i}{r} & 0 & 0 \\ 0 & 0 & -\frac{dN_i}{ds} \\ 0 & 0 & -N_i\frac{\cos\phi}{r} \\ -\frac{dN_i}{ds}\sin\phi & \frac{dN_i}{ds}\cos\phi & -N_i \end{bmatrix} \quad ; \quad \frac{dN_i}{ds} = \frac{dN_i}{d\xi}\frac{d\xi}{ds} = \frac{2}{L}\frac{dN_i}{d\xi} \tag{21}$$

Accounting for nonlinear response, nonlinear strain $\varepsilon^{NL} = (1/2)\left(dw/ds\right)^2$ have to be considered. Thus, it comes:

$$\boldsymbol{\varepsilon}^{NL} = \frac{1}{2}\mathbf{a}^T\,\mathbf{G}^T\,\mathbf{G}\,\mathbf{a} \quad ; \quad \mathbf{G} = \sum_{i=1}^{2} \begin{bmatrix} -\frac{dN_i}{ds}\sin\phi & 0 & 0 \\ 0 & \frac{dN_i}{ds}\cos\phi & 0 \end{bmatrix} \tag{22}$$

Elastoplastic and geometrically nonlinear analyses

From the virtual work principle, the incremental finite element equilibrium equations for geometrically nonlinear analysis, introducing thermal loads, and following and adapting the development of "Moita et al. (2018)", are given by:

$$\int_{{}^tA^e} \mathbf{B}^T\hat{\mathbf{D}}\,\mathbf{B}\ \Delta\mathbf{a}^e\ {}^tdA^e + \int_{{}^tA^e} \mathbf{G}^T\ (\hat{\sigma} - \hat{\sigma}^{th})\,\mathbf{G}\,\Delta\mathbf{a}^e\ {}^tdA^e = \mathbf{F}^e_{ext} - \mathbf{F}^e_{int} = \psi \tag{23}$$

and for elastoplastic analysis:

$$\int_{A^e} \mathbf{B}^T\hat{\mathbf{D}}^{ep}\,\mathbf{B}\,\Delta\mathbf{a}\,dA^e = \mathbf{F}^e_{ext} - \mathbf{F}^e_{int} = \psi \tag{24}$$

The linear and geometric stiffness matrices, external force vector (including distributed and concentrated transverse loads $\mathbf{f}$ and $\mathbf{F}_c$,) and internal force vector are given by:

$$\mathbf{K}^e_L = \int_{{}^tA^e} \mathbf{B}^T\,\hat{\mathbf{D}}\,\mathbf{B}\ \ {}^tdA^e \quad ; \quad \mathbf{K}^e_G = \int_{{}^tA^e} \mathbf{G}^T\,{}^t\hat{\boldsymbol{\sigma}}^L\mathbf{G}\,dA^e \quad ; \quad \mathbf{K}^e_0 = \int_{{}^tA^e} \mathbf{G}^T(-{}^t\hat{\boldsymbol{\sigma}}^{th})\,\mathbf{G}\,dA^e$$

$$\mathbf{F}^{e\ mec} = \int_{{}^0A^e} \mathbf{N}^T\mathbf{f}\ \ {}^0dA^e + 2\,\pi\,r\,F_c \quad ; \quad \mathbf{F}^{eth} = \int_{A^e} \mathbf{B}^T\tilde{\boldsymbol{\sigma}}^{th}\ dA^e \quad ; \quad \mathbf{F}^e_{\ int} = \int_{{}^tA^e} \mathbf{B}^T\left({}^t\hat{\boldsymbol{\sigma}}^L - {}^t\hat{\boldsymbol{\sigma}}^{th}\right){}^tdA^e$$

$${}^t\hat{\boldsymbol{\sigma}}^e = \begin{bmatrix} {}^t\mathbf{N}_s & 0 \\ 0 & {}^t\mathbf{N}_s \end{bmatrix} \quad ; \quad {}^t\mathbf{N}_s = {}^t\mathbf{N}^{mec}_s - {}^t\mathbf{N}^{th}_s \tag{25}$$

where ${}^tA^e = 2\,\pi\ {}^tr\ {}^tds = \pi\ {}^tr\ {}^tL\,d\xi$, and all the integrations are done by using only one Gauss point at $\xi = 0$ – reduction integration technique, "Zienkiewics et al. (1977)", allowing to obtain excellent results for both thin and thick axisymmetric plate/shells structures.

At any increment I, iteration i, we have:

$$\delta\mathbf{q}^{i} = (\mathbf{K}_{T})^{-1}\boldsymbol{\psi}^{i-1} \;;\; \delta\mathbf{q}^{i} = (\mathbf{K}_{ep})^{-1}\boldsymbol{\psi}^{i-1} \tag{26}$$

and at the end of the increment I is $\Delta\mathbf{q}^{I} = \Delta\mathbf{q}^{I-1} + \sum\delta\mathbf{q}^{i}$, when the residual force vector is very small, $\|\boldsymbol{\psi}\| < \|\mathbf{F}_{ext}\|\Delta$, where Δ is a predefined tolerance.

Using the Newton-Raphson incremental-iterative method, and implementing the automatic arc-length method for the case of snap-through occurrence, the incremental equilibrium path is obtained.

APPLICATIONS

Elastoplastic analysis of a simply supported isotropic circular plate, and pressure vessel.

The validation of the present model in the elastoplastic analysis is done by considering the proposed applications of "Popov et al. (1967)" and "Popov and Sharifi (1971)", where a simply supported circular plate and a pressure vessel with torispherical ends, both made of isotropic materials, subjected to a transverse and radial pressure load, respectively, are analysed. In Fig. 3a and Fig. 3b are presented the results obtained with the present model, using a layered model (20 layers), and a non-layered model (1 layer), and the results obtained by the authors cited before. A very good accuracy is observed. On other hand, as the layered model is better to simulate the stress distribution through the thickness, their results are more confident.

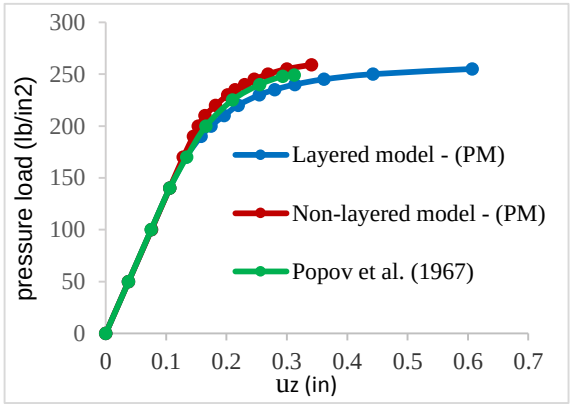

Figure 3a – Load-displacement path for a simply supported circular plate

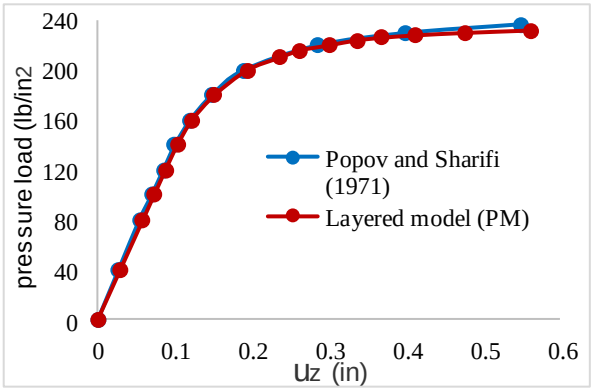

Figure 3b – Load-displacement path for a pressure vessel with torispherical ends

Nonlinear analyses of a FGM spherical cap under radial pressure.

A clamped spherical cap, Fig. 4, with radius of curvature R=2.286 m and thickness, half opening angle $\phi_0 = 35^o$, thickness h=0.0762 m, made of constituents zirconia and aluminium (E_m = 70.0 x10^9 N/m^2, ν_m =0.3, E_c =151.0 x 10^9 N/m^2, ν_c = 0.3), is considered. The nonlinear response of the spherical cap under a central point load and under a ring load analysed. For this type of structure under this type of loading, the occurrence of snap-through is possible, and thus the automatic arc-length method is used. First, to validate the present model, an application for an isotropic structure, proposed by "Surana (1982)", is performed. The results obtained using the present model and those obtained by "Surana (1982)" are shown in Fig. 5, and a good agreement is found.

Next, the present FGM spherical cap is investigated. The results are shown in Fig. 6a) for the case of central point load (r/a=0), and in Fig. 6b) for the case of ring load applied at coordinate ϕ=10º (r/a=0.3027). The occurrence of snap-through is observed for the last situation. Also it is observed that, for each load level, the displacement increases as the gradient index increases.

Pressure vessel with torispherical end, affected by temperature environment.

The static deformation of a FGM cylindrical pressure vessel with torispherical end is analysed. The constituents are Zirconia and Stainless Steel - ZrO2/SUS304, which material properties are function of temperature, and are given in Tab. 1, and shown in Fig 7a-b. This structure is represented in Fig. 8, where R=D_i=135 mm, t=1.27 mm, r_1=10.1 mm, and is subjected to an inner pressure load. The yield stress for SUS304 had been considered σ_{Ym} =400 MPa at 300 K.

First, to validate the present model, an elastoplastic analysis is performed for an isotropic material structure, considering the example presented in "Kirk and Gill (1974)", where is indicated a collapse pressure p_{col}=2.423 MPa, while the present model gives p_{col}=2.50 MPa.

Secondly, the effect of the temperature is investigated. The vessel is heating from 300 K to 350 K and from 300 K

to 400 K, respectively, with a through-the-thickness uniform temperature distribution. A nonlinear analysis is performed and the displacements at the apex, obtained by the thermal load are indicated in first line of Tab. 2, for the temperatures of 350 K and 400 K. Next, at final temperatures, the vessel is subjected to an internal pressure load from q_0=0 to q_0=2 MPa, for both previous cases. The displacements are given in second line of Tab. 2. It is observed, for this range of temperatures, the pure SUS304 metal vessel yields smaller deflections compared to the pure ZrO2 ceramic, and any other FGM vessels whose properties are a mixture of metal and ceramic. Also is observed that for any gradient index, the displacements due to mechanical load decrease as the temperatures increase, due to the initial stresses, although the effective Young modulus decreases. Thus, doing the same mechanical loading and considering that the vessel is stress free at final temperatures, the displacements increase (shown in the third line of Tab. 2), because of reduction of stiffeness.

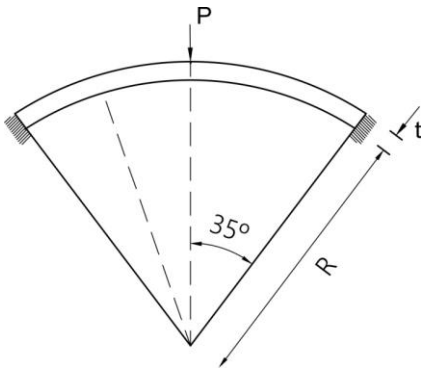

Figure 4 – Clamped spherical cap

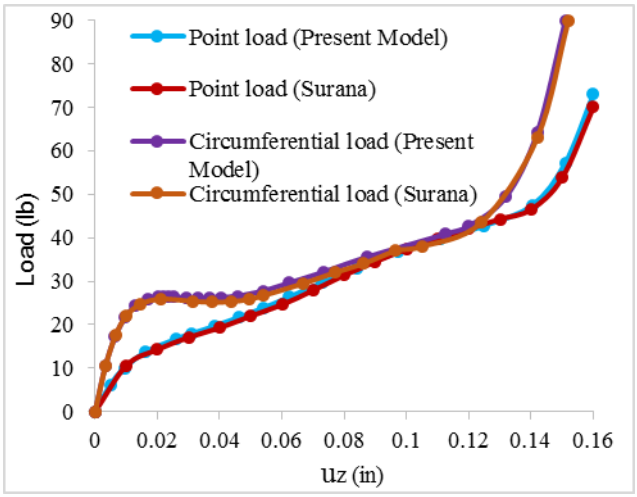

Figure 5 – Load-displacement paths for an isotropic spherical cap

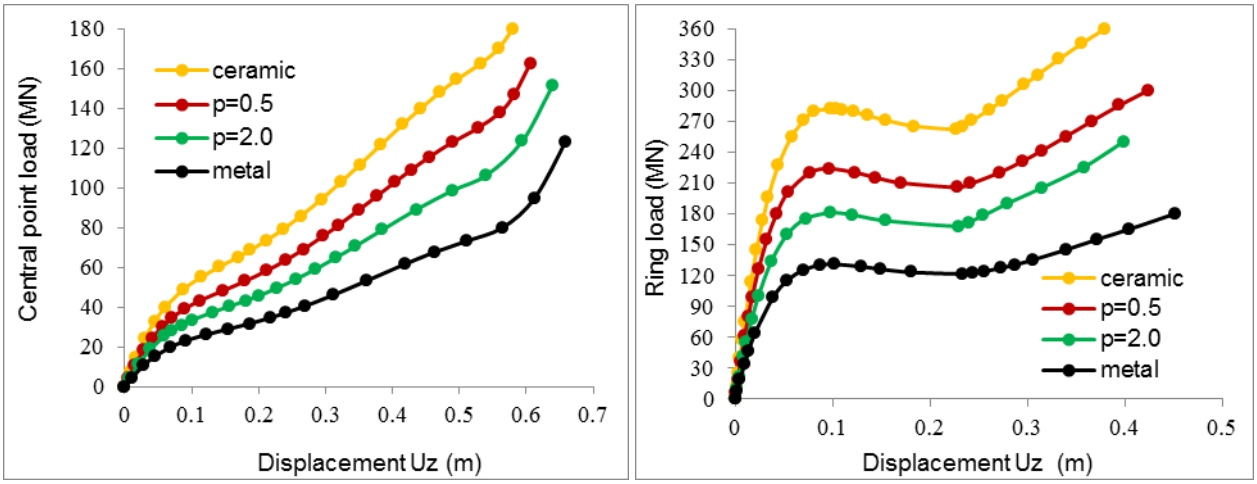

Figure 6a-b – Load-displacement paths for a FGM spherical cap under point load, and ring load.

Table 1 - Temperature-dependent coefficients for Zirconium Oxide and Stainless Steel.

Materials	Properties	P_0	P_{-1}	P_1	P_2	P_3
Zirconium Oxide (ZrO_2)	E (Pa)	$244.27\times10^{+9}$	0	-1.371×10^{-3}	1.214×10^{-6}	-3.681×10^{-10}
	ν	0.2882	0	1.133×10^{-4}	0	0
	α (1/K)	12.766×10^{-6}	0	-1.491×10^{-3}	-1.006×10^{-5}	-6.778×10^{-11}
Stainless Steel (SS304)	E (Pa)	$201.04\times10^{+9}$	0	3.079×10^{-4}	-6.534×10^{-7}	0
	ν	0.3262	0	-2.002×10^{-4}	3.797×10^{-7}	0
	α (1/K)	12.330×10^{-6}	0	8.086×10^{-4}	0	0

Next an elastoplastic analysis is performed at 300 K. The collapse pressures and the corresponding u_z displacement at the apex for different p-index are present in Tab. 3. For index p=0.5, the deformed shapes (enlarged 10 times), considering internal pressures of 2 MPa and 4.025 MPa (limit pressure) are shown in Fig. 9, with the plastic zone in yellow. In Fig. 10 is shown the corresponding elastoplastic load-displacement path, as well as for the case of 400 K, and

considering in the situation of stress free. The responses for the present application, considering different mechanical behaviours, at 300 K, are shown in Fig. 11. From Fig. 11, it is observed that real behaviour (GNL+EPL) gives a limit pressure greater than the limit pressure obtained using a pure elastoplastic analysis.

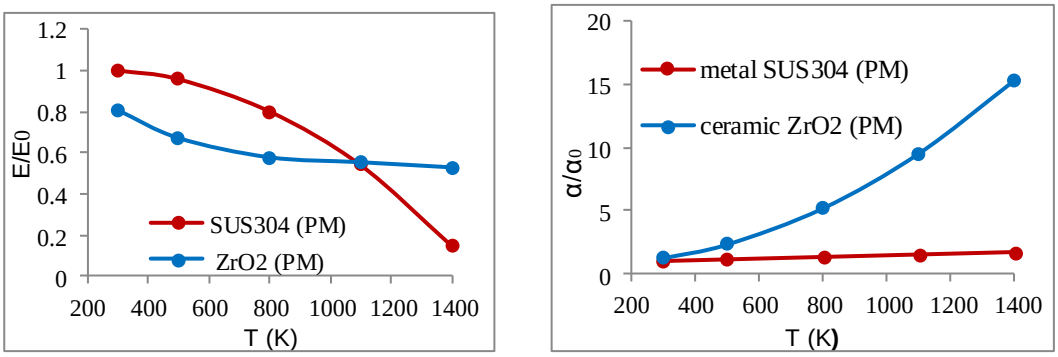

Figure 7 a-b - Young's modulus and coefficient of thermal expansion, as a function of temperature

Table 2 - Displacements (mm) at the apex of the pressure vessel for q_0=2 MPa. (* means no thermal load applied)

Temp (K)	Load	Ceramic	p=0.5	p=1.0	p=2.0	Metal
300	Mech.	0.2699*	0.2499*	0.2415*	0.2338*	0.2187*
350	Thermal	0.1889	0.1745	0.1666	0.1590	0.1458
	Mech.	0.2689	0.2467	0.2370	0.2283	0.2115
	Mech.	0.2838	0.2583	0.2477	0.2383	0.2199
400	Thermal	0.4120	0.3708	0.3490	0.3287	0.2964
	Mech.	0.2670	0.2419	0.2317	0.2225	0.2078
	Mech.	0.2973	0.2665	0.2540	0.2430	0.2217

Table 3 - Displacement (mm) and collapse pressure (MPa) in a FGM pressure vessel with torispherical end.

	p=0.5	p=1.0	p= 2.0	metal
Displacement u_z	1.287	1.289	1.220	1.181
Collapse pressure	4.025	4.070	4.105	4.205

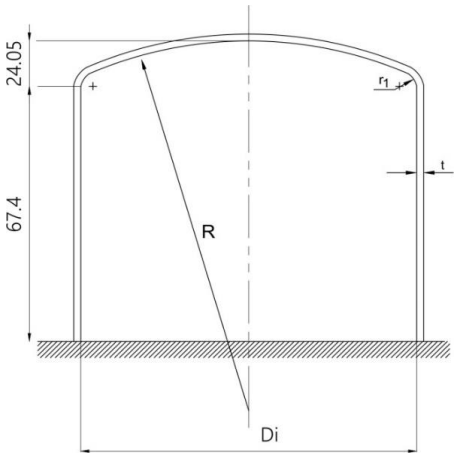

Figure 8 - Pressure vessel

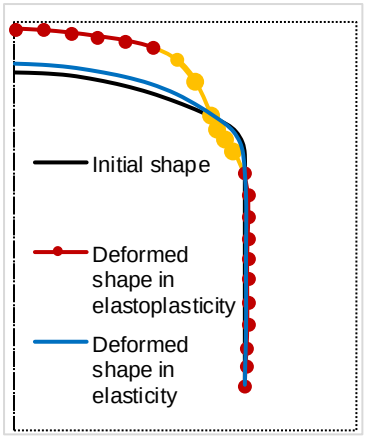

Figure 9 - Deformed shapes of the pressure vessel

Analysis of a toroidal shell, made of temperature dependent materials.

A toroidal FGM shell, shown in Fig. 12, is now analysed. The geometry is defined by r=254 mm, R=381 mm and thickness t=12.7 mm. The constituents are again Zirconia and Stainless Steel - ZrO2/SUS304, temperature-dependent materials, and the vessel is subjected to an inner radial pressure load. First, under a uniform pressure of $q_0 = 3.0$ MPa and ambient temperature T=300 K, the radial displacement for different p-index are obtained and shown in Fig 13. From Fig. 13 it is observed that the maximum and minimum deflections are for fully ceramic and fully metal respectively, as expected, because the Young modulus for ceramic is smaller than Young modulus for metal at 300 K. Also is observed that as p-index of FGM structure is increasing the displacements are decreasing.

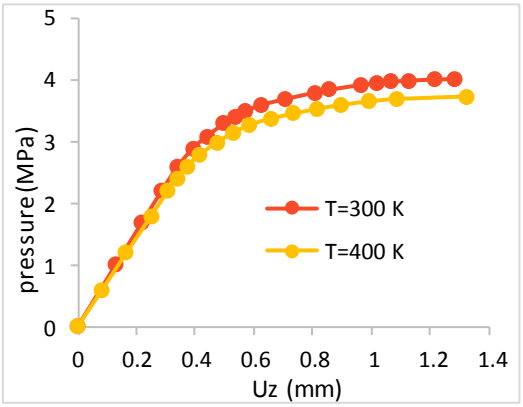

Figure 10 - Load-displacement paths in elastoplasticity.

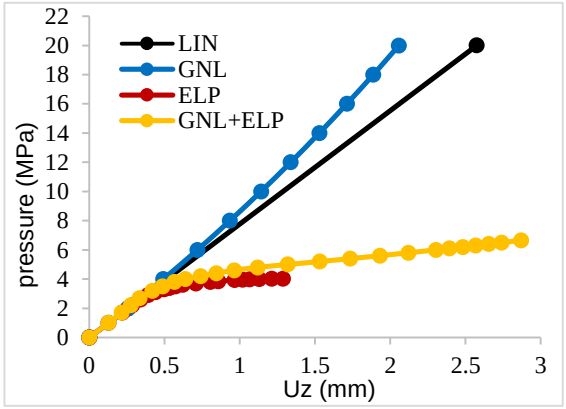

Figure 11 - Load-displacement paths for different deformation behaviours.

Next an elastoplastic analysis is performed, considering now the toroidal FGM shell for the case of gradient index p=1.0. Fig. 14 shows the original and deformed shapes for two different pressures at the temperature T=300 K, in which the displacements are amplified 100 times, and in yellow is shown the plastic zone. Fig. 15 shows the internal in-plane stress resultants distribution for load level q_0=6.0 MPa. The meridional forces are maximum at the inner circle and minimum at the outer circle.

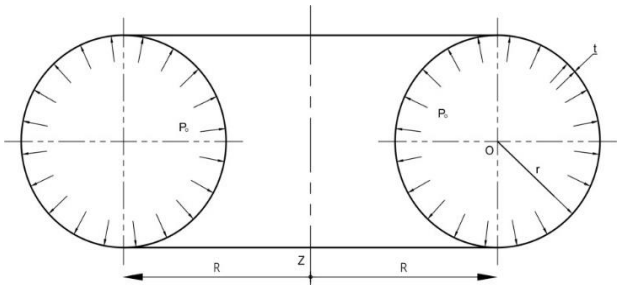

Figure 12 – Toroidal shell.

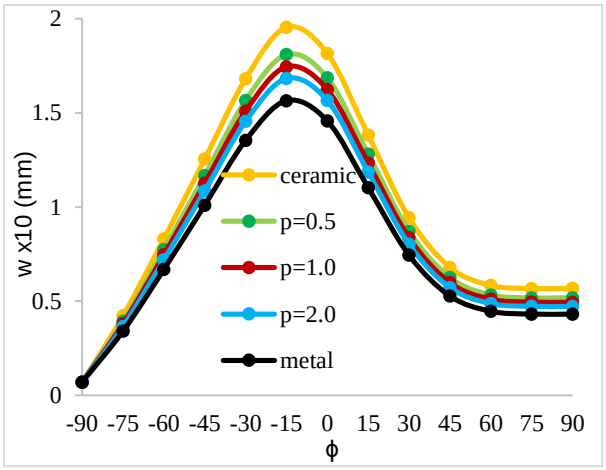

Figure 13 - Radial displacement in a FGM toroidal shell.

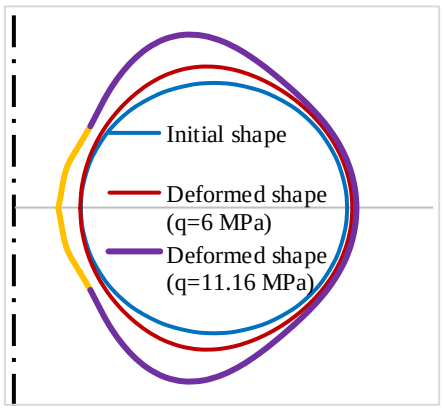

Figure 14 - Deformed shape of a FGM toroidal

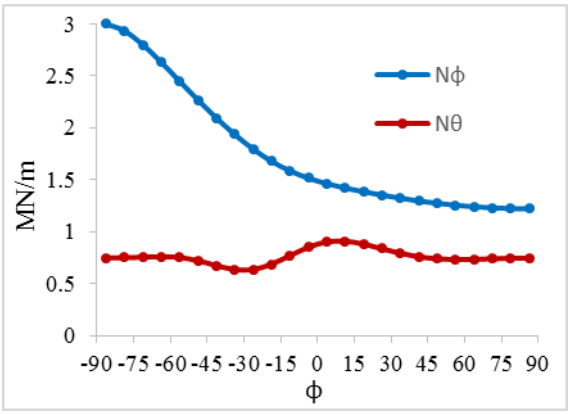

Figure 15 – Meridional and circumferential forces for q=3 MPa

CONCLUSIONS

A finite element model for elastoplasticity and geometrically nonlinear analyses of functionally graded (FGM) axisymmetric shells under axisymmetric loading and thermal environment is presented. The model is based on the first order shear deformation theory associated with a simple and fast conical frusta finite element with only 2 nodes and 3

degrees of freedom per node. The reduced number of finite elements necessary to model even complex structures, combined with the use of only twenty virtual layers to model the continuous variation of the mechanical properties through the thickness, yields in an extremely lower computational time for all FGM applications.

The effect of the temperature environment is investigated, and had been shown that for FGM structures made of temperature dependency properties, a great influence can be achieved. This influence is not only due to temperature itself, but also for the variation of the properties of ceramic and metal constituents as a function of temperature. Moreover, is important to note that the geometric nonlinear analysis and mainly the combined geometric and material nonlinear analysis play an important role to achieve the real solutions when large displacements have to be accounted.

A good to very good accuracy is found when the results obtained by the present model are compared with available solutions.

ACKNOWLEDGMENTS

This work was supported by FCT, Fundação para a Ciência e Tecnologia, through IDMEC, under LAETA, project UID/EMS/50022/2019, and also CNPq, CAPES and FAPERJ, from Brazil.

REFERENCES

Bao, G. and Wang L., 1995, "Multiple Cracking in Functionally Graded Ceramic/Metal Coatings", Internat. Journal of Solids and Structures, Vol. 32, pp. 2853–2871.

Gunes, R. and Reddy, J.N., 2008, "Nonlinear analysis of Functionally Graded circular plates", Internat. Journal of Structural Stability and Dynamics, Vol. 8 No. 1, pp. 131–159.

Kirk, A. and Gill, S.S., 1975, "The failure of torispherical ends of pressure vessels due to instability and plastic deformation - an experimental investigation", International Journal of Mechanical Science, Vol. 17, pp. 525-544.

Javaheri, R. and Eslami M.R., 2002, "Thermal buckling of functionally graded plates based on higher order theory", Journal of Thermal Stresses, Vol. 25, pp. 603–625

Jin, J.H., Paulino, G.H., Dodds Jr, R.H., 2003, "Cohesive fracture modeling of elastic–plastic crack growth in functionally graded materials", Engineering Fracture Mechanics, Vol. 70, No. 14, pp. 1885–912.

Li, X.Y., Ding, H.J., Chen, W.Q., 2008, "Elasticity solutions for a transversely isotropic functionally graded circular plate subject to an axisymmetric transverse load qr^k", International Journal of Solids and Structures, Vol. 45, pp. 191-210.

Ma, L., Deng, C., Ou, Z., 2008, "Nonlinear bending of FGM circular plates with temperature-dependent properties", Materials Science Forum, Vols. 575-578, pp. 1020-1024.

Moita, J.S., Araújo, A.L., Mota Soares, C.M., Mota Soares, C.A., Herskovits, J., 2016, "Material and geometric nonlinear analysis of functionally graded plate-shell type structures", Applied Composite Materials, Vol. 23, No. 4, pp. 537–554.

Moita, J.S., Araújo, A.L., Correia, V.F., Mota Soares, C.M., Herskovits, J., 2018, "Buckling and nonlinear response of functionally graded plated under thermo-mechanical loading", Composite Structures, Vol. 202, pp. 719–730.

Nayak, G.C, Zienckiewics, O.C., 1972, "Elastoplastic stress analysis. A generalization for various constitutive relations including strain softening", International Journal for Numerical Methods in Engineering, Vol. 5, pp. 113-135.

Popov, E.P., Khojesteh-Bakht, M., Yaghmai, S., 1967, "Analysis of elastic-plastic circular plates", Journal of Engineering Mechanical Division, Vol. 93, No. 6, pp. 49-66.

Popov, E.P. and Sharifi P., 1971, "A refined curved element for thin shells of revolution", International Journal for Numerical Methods in Engineering, Vol. 3, pp. 495-508.

Reddy, J.N., Wang C.M., Kitipornchа, S., 1999, "Axisymmetric bending of functionally graded circular and annular plates", European Journal of Mechanics - A/Solids, Vol. 18, pp. 185-199.

Surana, K.S., 1982, "Geometrically nonlinear formulation for the axisymmetric shell elements", Int. Journal for Numer. Meth. in Engineering, Vol. 18, pp. 477-502.

Zhang D.G., Zhou H.M., 2015, "Nonlinear bending analysis of FGM circular plates based on physical neutral surface and higher-order shear deformation theory", Aerospace Science and Technology, http://dx.doi.org/10.1016/j.ast.2014.12.016

Zienkiewics, O.C., Bauer, J., Morgan, K., Onate, E., 1977, "A simple and efficient element for axisymmetric shells", International Journal for Numerical Methods in Engineering, Vol. 11, pp. 1545 - 1558.

RESPONSIBILITY NOTICE

The authors are the only responsible for the printed material included in this paper.